

## Experimental Observation of Anisotropic Adler-Bell-Jackiw Anomaly in Type-II Weyl Semimetal $\text{WTe}_{1.98}$ Crystals at the Quasiclassical Regime

Yang-Yang Lv,<sup>1</sup> Xiao Li,<sup>2</sup> Bin-Bin Zhang,<sup>1</sup> W. Y. Deng,<sup>2</sup> Shu-Hua Yao,<sup>1,\*</sup> Y. B. Chen,<sup>2,†</sup> Jian Zhou,<sup>1,‡</sup> Shan-Tao Zhang,<sup>1</sup> Ming-Hui Lu,<sup>1</sup> Lei Zhang,<sup>4</sup> Mingliang Tian,<sup>3,4</sup> L. Sheng,<sup>2,3</sup> and Yan-Feng Chen<sup>1,3</sup>

<sup>1</sup>National Laboratory of Solid State Microstructures & Department of Materials Science and Engineering, Nanjing University, Nanjing, Jiangsu 210093, China

<sup>2</sup>National Laboratory of Solid State Microstructures & Department of Physics, Nanjing University, Nanjing, Jiangsu 210093, China

<sup>3</sup>Collaborative Innovation Center of Advanced Microstructure, Nanjing University, Nanjing, Jiangsu 210093, China

<sup>4</sup>High Magnetic Field Laboratory, Chinese Academy of Sciences, Hefei, Anhui 230031, China

(Received 27 September 2016; revised manuscript received 22 December 2016; published 3 March 2017)

The asymmetric electron dispersion in type-II Weyl semimetal theoretically hosts anisotropic transport properties. Here, we observe the significant anisotropic Adler-Bell-Jackiw (ABJ) anomaly in the Fermi-level delicately adjusted  $\text{WTe}_{1.98}$  crystals. Quantitatively,  $C_W$ , a coefficient representing the intensity of the ABJ anomaly along the  $a$  and  $b$  axis of  $\text{WTe}_{1.98}$  are 0.030 and 0.051  $\text{T}^{-2}$  at 2 K, respectively. We found that the temperature-sensitive ABJ anomaly is attributed to a topological phase transition from a type-II Weyl semimetal to a trivial semimetal, which is verified by a first-principles calculation using experimentally determined lattice parameters at different temperatures. Theoretical electrical transport study reveals that the observation of an anisotropic ABJ along both the  $a$  and  $b$  axes in  $\text{WTe}_{1.98}$  is attributed to electrical transport in the quasiclassical regime. Our work may suggest that electron-doped  $\text{WTe}_2$  is an ideal playground to explore the novel properties in type-II Weyl semimetals.

DOI: 10.1103/PhysRevLett.118.096603

The Adler-Bell-Jackiw (ABJ) anomaly is a remarkable phenomenon that originates from the breaking of chiral symmetry in the massless Weyl fermion under quantum fluctuation [1–6]. Previously, the ABJ anomaly was mainly observed in high-energy particle physics [1,2,7], while it was recently observed in Weyl semimetals, for example, TaAs, NbAs, and TaP, etc. [8–12]. In these materials, negative magnetoresistance (MR) due to ABJ anomaly can be observed at low temperatures when the magnetic field is parallel to the electric field. And this negative MR vanishes when the magnetic field is misaligned with respect to the electric field, or when the temperature is above a threshold value.

The latest progress in this field is the extension of the Weyl semimetal to a type-II Weyl semimetal in which the effective electron dispersion relationship breaks the honored Lorentz invariance [13–15]. Except for the Fermi arc at the Fermi surface, a remarkable fingerprint of type-II Weyl semimetals is the anisotropic transport properties, such as the anisotropic ABJ anomaly. Currently, several angle-resolved photoemission spectroscopy works have claimed to observe the Fermi arc in type-II Weyl semimetals, such as  $\text{WTe}_2$  [16–19],  $\text{MoTe}_2$  [20–25], and  $\text{LaAlGe}$  [26]. In a recent work, Wang *et al.*, reported the observation of negative magnetoresistance along the  $b$  axis in electrical-gated  $\text{WTe}_2$  few-layered samples [27]. A natural question is can we dope electrons into a  $\text{WTe}_2$  crystal to observe the ABJ anomaly. Obviously, an electron-doped  $\text{WTe}_2$  crystal has a permanent ABJ anomaly rather than a temporary one under electrical gating [27].

In this Letter, we report the evidence of an anisotropic ABJ anomaly in a type-II Weyl semimetal: Fermi-level, delicately adjusted  $\text{WTe}_{1.98}$  crystals. We found that a temperature-sensitive ABJ anomaly in the  $\text{WTe}_{1.98}$  crystal is attributed to a topological phase transition of the type-II Weyl semimetal phase in  $\text{WTe}_{1.98}$  converting to a topologically trivial semimetal at a high temperature ( $\sim 60$  K), which is verified by first-principles calculation using experimentally determined lattice parameters at different temperatures. Theoretical electrical transport study reveals that the observation of an anisotropic ABJ anomaly along both the  $a$  and  $b$  axis is attributed to the electrical transport at the quasiclassical regime, rather than an ultraquantum regime reported in the work of Wang [27].

We delicately synthesized a series of Te-deficient  $\text{WTe}_{2-\delta}$  ( $\delta$  is varied from 0.144 to 0.011) single crystals by the postannealing described in the Supplemental Material (SM) [28]. Theoretically, the position of Weyl points is about 60 meV above Fermi energy in the stoichiometric  $\text{WTe}_2$  [13,28]. In the experiment, we can observe the ABJ anomaly only in samples with  $\delta$  around 0.02. In the SM [28], the shift of Fermi energy in  $\text{WTe}_{1.98}$ , determined by a comparison between carrier concentration and integrated electron density of state, is quite approximately close to Weyl points.

As shown in Fig. 1(a), bulk  $\text{WTe}_2$  has a layered crystal structure. The x-ray diffraction (XRD) pattern of a  $\text{WTe}_2$  crystal is depicted in Fig. 1(b). Only the reflections of (002k) show up, suggesting that the crystals have a  $c$ -axis orientation. The full-width at half maximum of (002) pole is as small

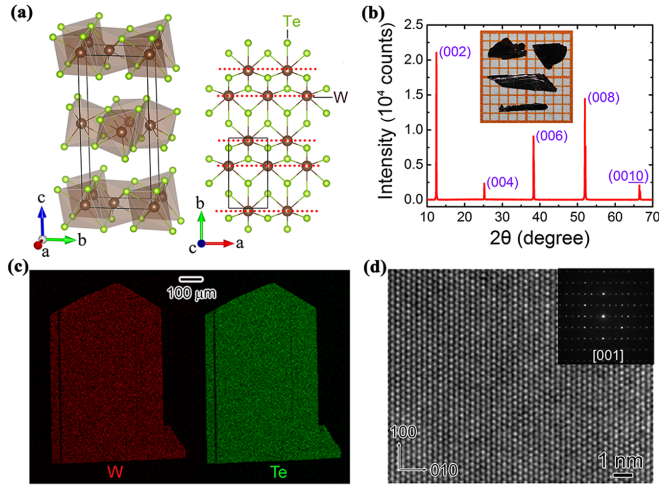


FIG. 1. Structural characterizations of  $\text{WTe}_2$  single crystals. (a) Crystal structure of  $\text{WTe}_2$ : a 3D perspective view along the  $a$  axis and a 2D projection along the  $c$  axis. W-W chains (highlighted by red-dashed line) are formed along the  $a$  axis. (b) The XRD patterns of representative  $\text{WTe}_2$  single crystal. The inset is a typical photograph of the as-grown  $\text{WTe}_2$  single crystals. (c) W (red) and Te (green) element mapping images of  $\text{WTe}_2$  single crystal. (d) High resolution TEM image of the  $\text{WTe}_2$  single crystal. The inset is a selected area electron diffraction of  $\text{WTe}_2$  with the electron beam aligned along the  $c$  axis.

as  $0.08^\circ$ , which infers the high crystalline quality. Figure 1(c) plots the energy-dispersive spectroscopy mappings of W and Te elements, which indicate that the two elements (W and Te) are uniformly distributed in  $\text{WTe}_2$  crystals. High resolution transmission electron microscopy (TEM) and the corresponding selected area electron diffraction pictures [see Fig. 1(d)] prove that the as-grown  $\text{WTe}_2$  crystals have single crystalline quality at the atomic scale.

Because the ABJ anomaly can only be observed in  $\text{WTe}_{1.98}$ , we will focus on describing electrical transport data of  $\text{WTe}_{1.98}$  in the following paragraph.

The longitudinal resistivity  $\rho_{xx}$  of the  $\text{WTe}_{1.98}$  single crystals, with an electrical current along the  $a$  and  $b$  axis, are shown in Fig. 2. Figure 2(a) depicts the temperature-dependent resistivity  $\rho_{xx,a}$  under various magnetic fields aligned along the  $c$  axis, with electrical current along the  $a$  axis. In the absence of an external magnetic field, the resistivity exhibits a typical metallic behavior. But an insulatorlike behavior is observed at low temperature when the magnetic field is applied. The physical origin of metal-insulator transition in  $\text{WTe}_2$  is still under hot debate [44]. The resistivity behavior  $\rho_{xx,b}$  with electrical current along the  $b$  axis under the magnetic field is quite similar to that along the  $a$  axis [see Fig. 2(b)].

The angle- and field-dependent MR of  $\text{WTe}_{1.98}$  crystals under different temperatures, with both electrical current ( $\vec{j}$ ) and magnetic field ( $\vec{B}$ ) applied along either the  $a$  or  $b$  direction, are shown in Fig. 3. One can see from Fig. 3(a) that the negative MR reaches the maximum ( $-30\%$ ) at 2 K and

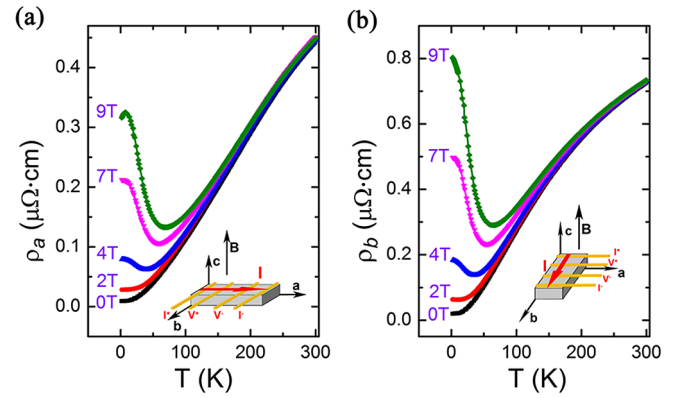


FIG. 2. Temperature-dependent resistivity along the  $a$  and  $b$  axis of electron-doped  $\text{WTe}_2$  crystals under varied magnetic fields aligned along the  $c$  axis. (a) The temperature-dependent resistivity  $\rho_{xx,a}$  with various magnetic fields along the  $c$  axis and current along the  $a$  axis. The inset is the schematic of the experiment. (b) The temperature-dependent resistivity  $\rho_{xx,b}$  with various magnetic fields along the  $c$  axis and current along the  $b$  axis. The inset is the schematic of the experiment.

vanishes at about 40 K under  $\vec{B} \parallel \vec{j} \parallel a$ -axis conditions. Figure 3(b) displays the field dependence of MR measured at 2 K on a different misalignment angle  $\theta$  (see the inset for the definition of  $\theta$ ). The MR reaches up to 1200% when the applied field is perpendicular to the current, but it changes to negative when  $\theta$  is between  $0^\circ$  and  $5^\circ$  [see the inset of Fig. 3(b)]. These features are quite similar to those observed in TaAs that is a prototypical type-I Weyl semimetal [8,9]. The similar MR behavior is also observed with  $\vec{B} \parallel \vec{j} \parallel b$ -axis conditions. As shown in Figs. 3(c) and 3(d), the negative MR of about  $-40\%$  is observed at 2 K and vanished at 30 K, and negative MR measured at 2 K is observed when the misalignment angle  $\theta$  is smaller than  $20^\circ$  [see the inset of Fig. 3(d)]. Comparing Fig. 3(a) to Fig. 3(c), the negative MR, measured at 9 T and 2 K, are  $-30\%$  and  $-40\%$  in the case of  $\vec{B} \parallel \vec{j} \parallel a$ -axis conditions and  $\vec{B} \parallel \vec{j} \parallel b$ -axis conditions, respectively. It, therefore, can be concluded that there is an obviously anisotropic negative MR in electron-doped  $\text{WTe}_2$  crystals. In the SM [28], we rule out the other possibilities—for example, the current-injecting effect, magnetism, and the ultraquantum effect—leading to the observed negative MR effect.

The ABJ anomaly induced negative MR in  $\text{WTe}_{1.98}$  crystals is further quantitatively analyzed by semiclassical formulas that have been successfully employed to analyze the ABJ anomaly in type-I Weyl semimetal [5,9]. The fitted formulas are

$$\sigma(B) = (1 + C_W B^2)\sigma_{WAL} + \sigma_N, \quad (1)$$

$$\sigma_{WAL} = \sigma_o + a\sqrt{B}, \quad (2)$$

where  $\sigma_{WAL}$  is the conductivity from weak antilocalization corrections associated with spin-orbit coupling and  $\sigma_N$  comes from conventional Fermi surface contributions except for Weyl points. The most important term in the

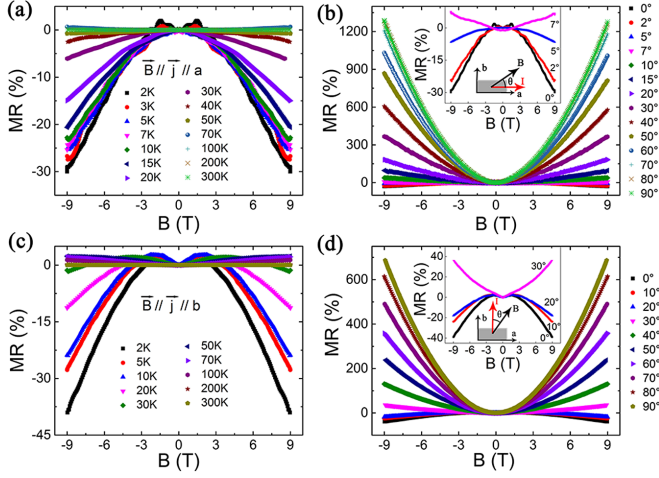


FIG. 3. Magnetic-field-dependent magnetoresistance of electron-doped  $\text{WTe}_2$  under different magnetic field directions and different temperatures. (a) The relationship between MR and the magnetic field of  $\text{WTe}_2$  single crystal measured at various temperatures, with  $\vec{B} \parallel \vec{j} \parallel a$  conditions. (b) The relationship between the MR of  $\text{WTe}_2$  and magnetic field under different  $\theta$  angles measured at 2 K with current along the  $a$  axis.  $\theta$  changing from  $0^\circ$  to  $90^\circ$  corresponds to magnetic field tilted from the  $a$  to the  $b$  axis. The inset shows the negative MR when  $\theta$  is tilted from  $0^\circ$  to  $5^\circ$ . (c) The relationship between MR and the magnetic field of a  $\text{WTe}_2$  single crystal measured at various temperatures, with  $\vec{B} \parallel \vec{j} \parallel b$  conditions. (d) The relationship between the MR of  $\text{WTe}_2$  and magnetic field under different  $\theta$  angles measured at 2 K with current along the  $b$  axis.  $\theta$  changing from  $0^\circ$  to  $90^\circ$  corresponds to the magnetic field tilted from the  $b$  to the  $a$  axis. The inset shows the negative MR when  $\theta$  is tilted from  $0^\circ$  to  $20^\circ$ .

formula is  $C_W B^2$  with a positive constant  $C_W$ , originating from the ABJ anomaly. First, the negative MR along both the  $a$  axis and the  $b$  axis measured at 2 K can be well fitted [shown in Fig. 4(a)] with the fitting parameters summarized in Table I. The  $C_W$  in the  $a$  and  $b$  axis are 0.030 and

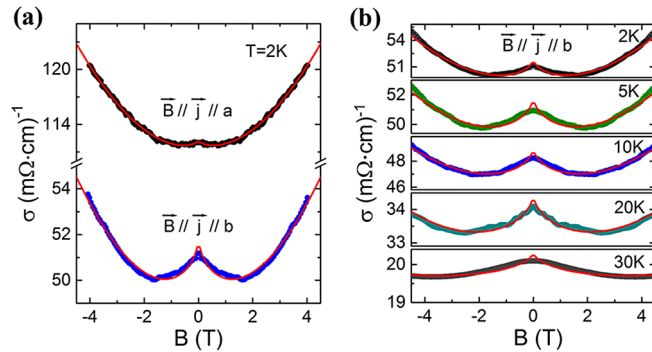


FIG. 4. Analysis of the ABJ anomaly in electron-doped  $\text{WTe}_2$  crystals under different temperatures and magnetic field directions. (a) The magnetoconductance of a  $\text{WTe}_2$  single crystal measured at 2 K under  $\vec{B} \parallel \vec{j} \parallel a$  or  $\vec{B} \parallel \vec{j} \parallel b$  conditions. The black or blue circles represent the experimental data and the red dashed lines are the fitted results. (b) The same theoretical fitting of the temperature-dependent ABJ anomaly with  $\vec{B} \parallel \vec{j} \parallel b$  conditions.

TABLE I. Fitting parameters of negative MR due to the ABJ anomaly of an electron-doped  $\text{WTe}_2$  crystal in the case of  $\vec{B} \parallel \vec{j} \parallel a$ -axis and  $\vec{B} \parallel \vec{j} \parallel b$ -axis conditions.

	$C_W$ ( $T^{-2}$ )	$a$ [ $T^{-0.5}$ ( $m\Omega \text{ cm}$ ) $^{-1}$ ]	$\sigma_0$ [( $m\Omega \text{ cm}$ ) $^{-1}$ ]	$\rho_0$ ( $m\Omega \text{ cm}$ )
$\vec{B} \parallel \vec{j} \parallel a$ axis	0.030	-0.231	1.709	0.287
$\vec{B} \parallel \vec{j} \parallel b$ axis	0.051	-0.115	1.502	0.103

0.051  $T^{-2}$  at 2 K, respectively, which obviously indicates that the ABJ anomaly along the  $b$  axis is more significant than that along the  $a$  axis. Second, the temperature-dependent negative MR, with  $\vec{B} \parallel \vec{j} \parallel b$ -axis conditions, are also fitted in Fig. 4(b). One can see the overall agreement between fitted and experimental results. The fitting parameters, summarized in the SM [28], suggest that the ABJ anomaly effect is decreased with increased temperature. Quantitatively,  $C_W$  is decreased from 0.051 to 0.007  $T^{-2}$  when the temperature is increased from 2 to 20 K. The temperature-sensitive ABJ anomaly is also observed in prototypical type-I Weyl semimetal TaAs [8,9].

As discussed in Fig. 3, the ABJ anomaly of  $\text{WTe}_{1.98}$  crystals can only be observed below 40 or 30 K, dependent on the direction. Here, we discuss two possible factors leading to the temperature-sensitive ABJ anomaly in  $\text{WTe}_2$ . The first factor is the possible temperature-dependent topological phase transition in  $\text{WTe}_2$ . In other words, the type-II Weyl semimetal phase in  $\text{WTe}_2$  is strongly dependent on lattice constants (equivalent to temperatures). First, we measured the temperature-dependent powder XRD of  $\text{WTe}_2$  at 35, 60, 100, 200, and 300 K. Then their crystal structures at these temperatures were determined by Rietveld refinement. Figure 5(a) displays the agreement between observed (crosses) and fitted (solid lines) diffraction patterns at 35 K. All the refined lattice constants are summarized in Table S2 in the SM [28], and they can be well linearly fitted, as shown in Fig. 5(b). Based on the linear fit, we then calculated the evolution of Weyl points in  $\text{WTe}_2$  crystal at different lattice constants from 0 to 130 K (details can be found in the SM [28]). Figure 5(c) shows two band crossing points (Weyl points) at 0 K, which is very similar to the result of Soluyanov [13]. In other words,  $\text{WTe}_2$  is a type-II Weyl semimetal at 0 K. However, at a higher temperature of 130 K [see Fig. 5(d)], there is an energy gap (about 1.9 meV) which indicates that  $\text{WTe}_2$  at 130 K is not a type-II Weyl semimetal any more. The whole evolution from the type-II Weyl semimetal to the trivial semimetal in  $\text{WTe}_2$  can be clearly seen in Fig. 5(e), in which we find that the separation distance between the two Weyl points decreases to almost zero at about 70 K, while at the same time, the obvious energy gap appears when the temperature exceeds about 70 K. Therefore, we can conclude that the  $\text{WTe}_2$  undergoes a topological phase transition from the type-II Weyl semimetal to the trivial one with the transition temperature of about

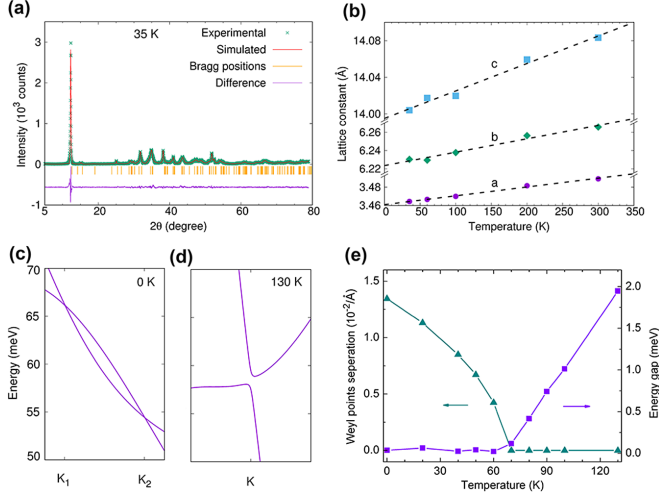


FIG. 5. Temperature-dependent lattice constants and Weyl-point evolutions at different temperatures in  $\text{WTe}_2$ . (a) Rietveld refinement of the x-ray diffraction data of polycrystalline  $\text{WTe}_2$  crystal at 35 K. Cross marks ( $\times$ ) and the red solid lines represent the experimental and Rietveld refinement results, respectively. The differences between the calculated and observed patterns are plotted at the bottom (purple line). The orange vertical lines indicate the calculated positions of the Bragg reflections for the proposed crystal structure. (b) Temperature-dependent lattice constants  $a$ ,  $b$ , and  $c$ . The dotted lines are the linear fittings of the experimental lattice constants. (c) Band structure of  $\text{WTe}_2$  with the lattice constants at 0 K. Two crossing points  $K_1$  and  $K_2$  are the two Weyl points. (d) Same as (c) but for the lattice constants at 130 K. A small energy gap appears and no Weyl points are found. (e) The whole evolutions of the separation distances between two Weyl points and the energy gaps of  $\text{WTe}_2$  at different temperatures from 0 to 130 K.

70 K. These calculations clearly demonstrate the highly sensitive Weyl state in  $\text{WTe}_2$  on the lattice constants (equivalent to the temperature). Thus, the above-mentioned temperature-sensitive ABJ anomaly should be attributed to topological phase transition in  $\text{WTe}_2$  under thermal perturbation. The second factor leading to the temperature-sensitive ABJ anomaly is the Fermi level changed by the thermal agitation. Based on current data, we cannot distinguish which factor is dominated to the temperature-sensitive ABJ anomaly in the  $\text{WTe}_2$  crystal.

In the following paragraphs, we will answer two important questions. How can we correlate the calculated electronic band structure with the observed ABJ anomaly in a semiquantitative or quantitative way? How do we reconcile our observation of the ABJ anomaly on both the  $a$  and  $b$  axis, while it is only observed along the  $b$  axis in electrical-gated  $\text{WTe}_2$  few-layered samples as reported [27]? We analyze the anisotropic chiral anomaly, which leads to the anisotropic negative longitudinal magnetoresistance. The general form of the Hamiltonian around a Weyl point is [13]

$$H(\vec{k}) = Ak_x + Bk_y + (ak_x + ck_y)\sigma_y + (bk_x + dk_y)\sigma_z + ek_z\sigma_x. \quad (3)$$

The Berry curvature is calculated to be

$$\vec{\Omega}_{n,k} = -\frac{n}{2g^3} (ad - bc) e\vec{k}, \quad (4)$$

where  $g = \sqrt{e^2k_z^2 + (ak_x + ck_y)^2 + (bk_x + dk_y)^2}$ ,  $n = \pm 1$  for  $n$ th band.

In the ultraquantum limit, the chiral anomaly is characterized by the ratio  $R$  around the Weyl point, defined as [13]

$$R = \frac{(Ak_x + Bk_y)^2}{g^2}. \quad (5)$$

Chiral anomaly and related negative magnetoresistance occur *only* in the direction with  $R > 1$  [13]. It is convenient to express  $R$  defined in Eq. (3) along the  $a$  or  $b$  axis as

$$R = \left( \frac{\lambda_+ + \lambda_-}{\lambda_+ - \lambda_-} \right)^2, \quad (6)$$

where  $\lambda_{\pm}$  are the slopes of the two energy dispersion curves at the Weyl point along the  $a$  or  $b$  axis. It is easy to find that  $R > 1$ , if the two slopes have the same sign, and  $R < 1$  otherwise. By using the data of the slopes around the two Weyl points obtained from our first principle calculation, we find  $R > 1$  occurs only along the  $b$  axis and  $R < 1$  along the  $a$  axis, as shown in Fig. S10 [28]. This means that in the ultraquantum regime, the chiral anomaly induced negative longitudinal magnetoresistance only happens along the  $b$  axis.

However, in the opposite classical limit, it is found that chiral anomaly induced negative magnetoresistance is isotropic [42], and so positive longitudinal magnetoconductivity is present along any arbitrary direction. The longitudinal conductivity  $\sigma_{uu}$  can be obtained based on the classical Boltzmann equation, incorporating the Berry curvature effect, as [42]

$$\sigma_{uu} = \sigma_{u,0} + \gamma_u B^2. \quad (7)$$

The expressions for  $\sigma_{u,0}$  and  $\gamma_u$  can be found in the Supplemental Material [28], the analysis shows that  $\gamma_u$  is isotropic for low magnetic fields and away from the band touch point ( $k = 0$ ).

The longitudinal magnetoresistance can be expressed as

$$\text{MR} = \frac{\rho - \rho_0}{\rho_0} = -\frac{\gamma_u B^2}{\sigma_{u,0} + \gamma_u B^2}. \quad (8)$$

We can see that the negative longitudinal magnetoresistance could occur along any arbitrary direction.

Thus one can expect that in the intermediate quasi-classical region, the negative magnetoresistance should exhibit a crossover from extreme anisotropy to isotropy. Theoretically, whether a system is in the ultraquantum limit or semiclassical limit is determined by the product of cyclotron frequency  $\omega_c$  and relaxation time  $\tau$ . The system is in the ultraquantum limit if  $\omega_c \tau \gg 1$ , and in the classical limit if  $\omega_c \tau \ll 1$  [4,41]. In our case,  $\omega_c \tau$  is found to be 0.51 under 5 T magnetic field. It suggests that our samples are

within the quasiclassical region, i.e., the crossover region from the ultraquantum limit to the semiclassical limit. Therefore, it is reasonable to observe in our experiment that nonvanishing but anisotropic negative longitudinal magnetoresistance occur along both the  $a$  and  $b$  axes. It should be mentioned that a recent theoretical work [42] also reported the isotropic ABJ anomaly in type-II Weyl semimetal. The main conclusion is quite consistent with our above discussions.

In summary, we experimentally observe the obviously anisotropic ABJ anomaly in Fermi-level delicately adjusted  $\text{WTe}_{1.98}$  crystal. The temperature-sensitive ABJ anomaly may be attributed to the topological phase transition of  $\text{WTe}_{1.98}$  under thermal agitation. Theoretical electrical transport study reveals that an anisotropic but finite ABJ anomaly can be observed on both the  $a$  and  $b$  axis in type-II Weyl semimetal at the quasiclassical regime.

We would like to acknowledge the financial support from the National Natural Science Foundation of China (No. 51472112, No. 51032003, No. 11374140, No. 11374149, No. 10974083, No. 11004094, No. 11134006, No. 11474150, and No. 11174127), and the major State Basic Research Development Program of China (973 Program) (No. 2015CB921203, No. 2013CB632702). Y.-Y.L acknowledges the financial support from the Graduate Innovation Fund of Nanjing University (No. 2015CL11). S.H.Y. acknowledges the enlightening discussion with Dr. Maxim Avdeev at ANSTO on Rietveld analysis of powder XRD results. The use of the computational resources in the High Performance Computing Center of Nanjing University for this work is also acknowledged.

Y.-Y. L., X. L., and B.-B. Z. contributed equally to this work.

\*Corresponding author.  
shyao@nju.edu.cn

†Corresponding author.  
ybchen@nju.edu.cn

‡Corresponding author.  
zhoujian@nju.edu.cn

- [1] M. E. Peskin and D. V. Schroeder, *An Introduction to Quantum Field Theory* (Westview Press, Boulder, 1995).
- [2] A. Zee, *Quantum Field Theory in a Nutshell* (Princeton University Press, Princeton, 2003), 2nd ed.
- [3] P. Hosur and X. L. Qi, *C.R. Phys.* **14**, 857 (2013).
- [4] H. B. Nielsen and M. Ninomiya, *Phys. Lett. B* **130**, 389 (1983).
- [5] H.-J. Kim, K.-S. Kim, J.-F. Wang, M. Sasaki, N. Satoh, A. Ohnishi, M. Kitaura, M. Yang, and L. Li, *Phys. Rev. Lett.* **111**, 246603 (2013).
- [6] J. Xiong, S. K. Kushwaha, T. Liang, J. W. Krizan, M. Hirschberger, W. D. Wang, R. J. Cava, and N. P. Ong, *Science* **350**, 413 (2015).
- [7] A. M. Bernstein and B. R. Holstein, *Rev. Mod. Phys.* **85**, 49 (2013).
- [8] C.-L. Zhang *et al.*, *Nat. Commun.* **7**, 10735 (2016).
- [9] X. C. Huang *et al.*, *Phys. Rev. X* **5**, 031023 (2015).
- [10] X. J. Yang, Y. P. Li, Z. Wang, Y. Zheng, and Z. A. Xu, [arXiv:1506.03190](https://arxiv.org/abs/1506.03190).
- [11] F. Arnold *et al.*, *Nat. Commun.* **7**, 11615 (2016).
- [12] J. H. Du *et al.*, *Sci. China Phys. Mech. Astron.* **59**, 657406 (2016).
- [13] A. A. Soluyanov, D. Gresch, Z. J. Wang, Q. S. Wu, M. Troyer, X. Dai, and B. A. Bernevig, *Nature (London)* **527**, 495 (2015).
- [14] T. R. Chang *et al.*, *Nat. Commun.* **7**, 10639 (2016).
- [15] Y. Sun, S.-C. Wu, M. N. Ali, C. Felser, and B. H. Yan, *Phys. Rev. B* **92**, 161107(R) (2015).
- [16] F. Y. Bruno *et al.*, *Phys. Rev. B* **94**, 121112(R) (2016).
- [17] C. L. Wang *et al.*, *Phys. Rev. B* **94**, 241119(R) (2016).
- [18] Y. Wu, D. X. Mou, N. H. Jo, K. W. Sun, L. Huang, S. L. Bud'ko, P. C. Canfield, and A. Kaminski, *Phys. Rev. B* **94**, 121113(R) (2016).
- [19] B. J. Feng *et al.*, *Phys. Rev. B* **94**, 195134 (2016).
- [20] K. Deng *et al.*, *Nat. Phys.* **12**, 1105 (2016).
- [21] J. Jiang *et al.*, [arXiv:1604.00139](https://arxiv.org/abs/1604.00139).
- [22] A. J. Liang *et al.*, [arXiv:1604.01706](https://arxiv.org/abs/1604.01706).
- [23] L. Huang *et al.*, *Nat. Mater.* **15**, 1155 (2016).
- [24] A. Tamai *et al.*, *Phys. Rev. X* **6**, 031021 (2016).
- [25] I. Belopolski *et al.*, *Phys. Rev. B* **94**, 085127 (2016).
- [26] S.-Y. Xu *et al.* [arXiv:1603.07318](https://arxiv.org/abs/1603.07318).
- [27] Y. J. Wang *et al.*, *Nat. Commun.* **7**, 13142 (2016).
- [28] See Supplemental Material at <http://link.aps.org/supplemental/10.1103/PhysRevLett.118.096603>, which includes Refs. [4,8,9,13,29–43], for details.
- [29] Y.-Y. Lv *et al.*, *Sci. Rep.* **6**, 26903 (2016).
- [30] M. N. Ali, L. Schoop, J. Xiong, S. Flynn, Q. Gibson, M. Hirschberger, N. P. Ong, and R. J. Cava, *Europhys. Lett.* **110**, 67002 (2015).
- [31] A. B. Pippard, *Magnetoresistance in Metals* (Cambridge University Press, Cambridge, 1989).
- [32] B. H. Toby, *J. Appl. Crystallogr.* **34**, 210 (2001).
- [33] W. G. Dawson and D. W. Bullett, *J. Phys. C* **20**, 6159 (1987).
- [34] G. Kresse and J. Hafner, *Phys. Rev. B* **48**, 13115 (1993).
- [35] G. Kresse and J. Furthmüller, *Comput. Mater. Sci.* **6**, 15 (1996).
- [36] P. E. Blöchl, *Phys. Rev. B* **50**, 17953 (1994).
- [37] G. Kresse and D. Joubert, *Phys. Rev. B* **59**, 1758 (1999).
- [38] J. P. Perdew, K. Burke, and M. Ernzerhof, *Phys. Rev. Lett.* **77**, 3865 (1996).
- [39] I. Pletikoscic, M. N. Ali, A. V. Fedorov, R. J. Cava, and T. Valla, *Phys. Rev. Lett.* **113**, 216601 (2014).
- [40] N. W. Ashcroft and N. D. Mermin, *Solid State Physics* (Thomson Learning Inc., New York, 1976).
- [41] A. A. Abrikosov, *Fundamentals of the Theory of Metals* (Elsevier Science Publishers, Amsterdam, 1988).
- [42] G. Sharma *et al.*, [arXiv:1608.06625](https://arxiv.org/abs/1608.06625).
- [43] G. Sharma, P. Goswami, and S. Tewari, *Phys. Rev. B* **93**, 035116 (2016).
- [44] M. N. Ali *et al.*, *Nature (London)* **514**, 205 (2014).